ACS Sustainable Chemistry & Engineering

Research Article

Cite This: ACS Sustainable Chem. Eng. 2018, 6, 16205−16218

pubs.acs.org/journal/ascecg

Hydrodeoxygenation of Isoeugenol over Alumina-Supported Ir, Pt, and Re Catalysts

Moldir Alda-Onggar,[†] Päivi Mäki-Arvela,[†] Kari Eränen,[†] Atte Aho,[†] Jarl Hemming,[†] Petriina Paturi,[‡] Markus Peurla,[§] Marina Lindblad,[∥] Irina L. Simakova,[⊥] and Dmitry Yu. Murzin*[,†]

[†]Johan Gadolin Process Chemistry Centre, Åbo Akademi University, Turku, Finland

[‡]Wihuri Physical Laboratory, Department of Physics and Astronomy, University of Turku, Turku, Finland

[§]Laboratory of Electron Microscopy, University of Turku, Turku, Finland

[∥]Neste Corporation, Porvoo, Finland

[⊥]Boreskov Institute of Catalysis, Novosibirsk, Russia

Supporting Information

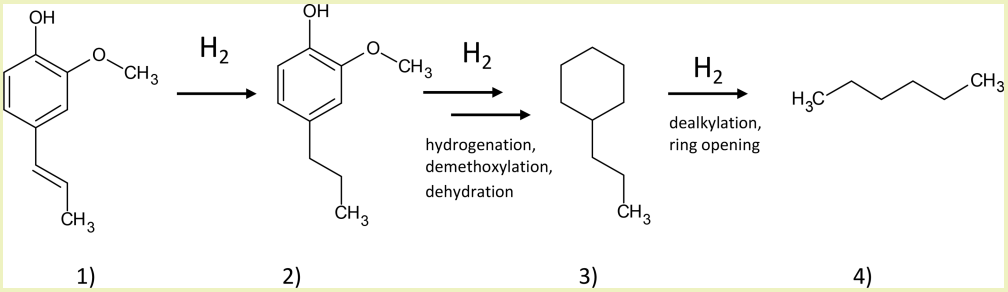

ABSTRACT: Hydrodeoxygenation (HDO) of isoeugenol (IE) was investigated using bimetallic iridium−rhenium and platinum−rhenium catalysts supported on alumina in the temperature and pressure ranges of 200−250 °C and 17−40 bar in nonpolar dodecane as a solvent. The main parameters were catalyst type, hydrogen pressure, and initial concentration. Nearly quantitative yield of the desired product, propylcyclohexane (PCH), at complete conversion in 240 min was obtained with Ir−Re/Al_2O_3 prepared by the deposition−precipitation method using 0.1 mol/L IE initial concentration. High iridium dispersion together with a modification effect of rhenium provided in situ formation of the IrRe active component with reproducible catalytic activity for selective HDO of IE to PCH. The reaction rate was shown to increase with the increasing initial IE concentration promoting also HDO and giving a higher liquid phase mass balance. Increasing hydrogen pressure benefits the PCH yield.

KEYWORDS: *Hydrodeoxygenation, Bimetallic catalyst, Isoeugenol*

INTRODUCTION

Due to depleting fossil resources, such energy sources as bio-oil from biomass, wood or woody crops, and agricultural wastes[1,2] are nowadays considered as viable alternatives. In contrast to fossil fuels such as crude oil, natural gas, and coal, biomass is renewable, affecting the carbon cycle.[1] Bio-oils, typically produced via fast pyrolysis, are dark hazel colored liquids of complex structure with a strong smoke-filled scent.[3] Bio-oils are complex mixtures achieved by depolymerization and fragmentation of lignocellulosic biomass. Due to their high oxygen content and instability, bio-oils cannot be used as fuel directly, requiring upgrading.[3,4]

Investigation of bio-oil upgrading via hydrodeoxygenation (HDO) is challenging due to the complex structure of bio-oil and its instability. HDO of different model compounds, such as guaiacol,[5] vanillin,[6] anisole,[7] and simulated bio-oil,[8] has been used to get fundamental insight into HDO. HDO of phenolic compounds over heterogeneous catalysts was recently also summarized by Mäki-Arvela and Murzin.[9] HDO of phenolic compounds has been stated to occur via hydrogenation and hydrogenolysis happening on the metal sites, whereas dehydration, isomerization, alkylation, and condensation proceed on the acid sites.[10] Despite the fact that acidic conditions accelerate hydrodeoxygenation of model compounds, the use of acidic catalysts, however, leads to coke formation and further catalyst deactivation.[11]

In this work, isoeugenol was used as a model compound to study HDO because it was found as an important constituent of bio-oil from pine.[12] Most of the work reported in the literature has not considered (iso)eugenol as a model compound. Eugenol and isoeugenol differ in their structures in a way that the latter compound exhibits a double bond at

Received: June 28, 2018
Revised: September 1, 2018
Published: October 15, 2018

Table 1. Literature Data of Eugenol HDO over Different Metal-Supported Catalysts

Entry	Mildly acidic catalyst	Solvent	Conversion of eugenol (%)	Operational conditions (reaction duration, temperature, pressure)	Main products (selectivity %)	ref
1	Pd/Al_2O_3	hexadecane	100	1 h, 250 °C, and 30 bar	Dihydroeugenol (46%), 1-Hydroxyl-4-propylbenzene (20%), Propylcyclohexane (20%)	11
2	Ru/Al_2O_3	hexadecane	100	1 h, 250 °C, and 30 bar	Dihydroeugenol (59%), 1-Hydroxy-2-methoxy-4-methylbenzene (13%)	11
3	Pt/Al_2O_3	hexadecane	100	1 h, 250 °C, and 30 bar	Dihydroeugenol (92%), 1-Hydroxyl-4-propylbenzene (2%)	11
4	Ni/γ-Al_2O_3	octane	99	16 h, 300 °C, and 50 bar	Hydrocarbons (77%)	21
5	Raney-Ni and H-ZSM-5	methanol, water	97	7 h, 220 °C, 5 bar	Propylcyclohexane (86%)	18
6	Co/TiO_2	*n*-dodecane	100	2 h, 200 °C, and 12 bar	4-Propylcyclohexanol (100%)	20
7	Pd/C	hexadecane	100	1 h, 250 °C, and 30 bar	1-Hydroxy-2-methoxy-propylcyclohexane (89%)	11
8	Ru/C	hexadecane	100	1 h, 250 °C, and 30 bar	Dihydroeugenol (77%), 1-Hydroxyl-4-propylbenzene(6%)	11
9	Pt/C	hexadecane	100	1 h, 250 °C and 30 bar	1-Hydroxy-2-methoxy-propylcyclohexane (95%)	11
10	4 wt % Ru/C	hexadecane	100, ($C_{0,r}$ = 232.6 mol/m^3)	3 h, 275 °C, and 40 bar	Dihydroeugenol (34%), 4-Propylcyclohexanol (30%), Propylcyclohexane (17%)	13
11	4 wt % Ru/C	hexadecane	100, ($C_{0,r}$ = 238.4 mol/m^3)	3 h, 275 °C, and 50 bar	Dihydroeugenol (39%), 4-Propylcyclohexanol (32%), Propylcyclohexane (22%)	13
12	4 wt % Ru/C	hexadecane	100, ($C_{0,r}$ = 244.2 mol/m^3)	3 h, 275 °C, and 60 bar	Dihydroeugenol (43%), 4-Propylcyclohexanol (31%), Propylcyclohexane (24%)	13
13	4 wt % Ru/C	hexadecane	100, ($C_{0,r}$ = 241.3 mol/m^3)	3 h, 275 °C, and 70 bar	Dihydroeugenol (47%), 4-Propylcyclohexanol (29%), Propylcyclohexane (14%)	13
14	RuRe/multiwalled carbon nanotube	heptane	99.4	1 h, 200 °C, and 20 bar	Propylcyclohexane (62%)	17
15	5 wt % Pd/C + H-ZSM-5	water	–	4 h, 240 °C, and 50 bar	Hydrocarbons (72%), 4-Propylcyclohexanol	22
16	Pt/H-beta-300	dodecane[a]	100	4 h, 200 °C, and 30 bar	Propylcyclohexane (89%)	15

[a]Reactant isoeugenol.

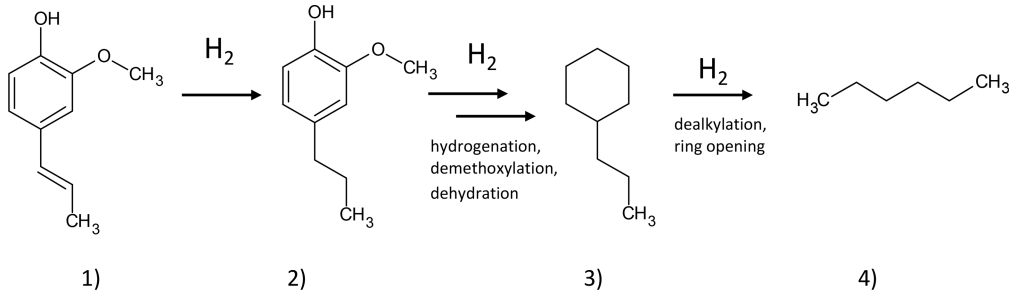

Figure 1. Reaction scheme for isoeugenol hydrodeoxygenation. Notation: (1) isoeugenol, (2) dihydroeugenol, (3) propylcyclohexane, and (4) hexane.

the C2 position in the propyl chain instead of C1. Eugenol HDO has been previously investigated over several types of catalysts (Table 1).[11,13−22] Transformations of eugenol, in the absence of any catalyst were also reported.[13] Isoeugenol (1) HDO (Figure 1) proceeds through initial hydrogenation producing dihydroeugenol (2) and isomerization and subsequent hydrogenolysis resulting in the cleaved methoxy ($-OCH_3$), allyl (e.g., $-C_2H_5$), and hydroxyl ($-OH$) groups.[14,15] Formation of hexane in HDO of isoeugenol has been added to Figure 1 because its formation was demonstrated in this work over $Ir-Re/Al_2O_3$ catalysts.

In HDO of eugenol palladium,[16] platinum, ruthenium, and nickel supported on γ-Al_2O_3[21] have been used as catalysts. Pd, Pt, and Ru on alumina resulted in complete conversion of eugenol, while HDO efficiency and formation of propylcyclohexane were rather limited. The best performing catalyst was Pd/Al_2O_3, giving 10% of propylcyclohexane (Table 1). On the other hand, high conversion (99%) and deoxygenation yield (77%) in HDO of eugenol was demonstrated using Ni/ γ-Al_2O_3.[21] Clearly, the metal type and operational conditions are the parameters determining the product distribution in eugenol HDO. Besides alumina, carbon is also an attractive support due to its high tolerance toward acidic environment and a possibility to recycle metals in the catalyst via burning carbon.[23] Pd/C and Pt/C catalysts gave in eugenol HDO products of hydrogenation, while Ru/C exhibited some minor hydrogenolysis as reported by Bjelic et al.[13] Recently, it was demonstrated that Pt supported on H-Beta zeolite was an efficient catalyst for HDO of isoeugenol giving propylcyclohexane as the main product with the selectivity of 89% at 100% conversion. It should, however, be noted that the liquid phase mass balance closure was only 61% due to the presence of an acidic catalyst.[15] It can be concluded that in eugenol HDO complete deoxygenation of eugenol is challenging over Pd, Ru, or Pt catalysts supported on alumina or carbon. Furthermore, Co/TiO_2 gave only partially deoxygenated propylcyclohexanol as the main product,[20] showing the importance of the metal and support selection for HDO of eugenol.

DOI: 10.1021/acssuschemeng.8b03035
ACS Sustainable Chem. Eng. 2018, 6, 16205−16218

The aim of this work was to study HDO of isoeugenol using Ir and Re supported on γ-Al_2O_3 as catalysts. According to our knowledge, these types of bimetallic catalysts have not yet been applied in eugenol HDO. However, they have been demonstrated to be active in HDO of furylmethane to produce aviation turbine fuel.[24] According to the literature, Ir is active for C−O bond hydrogenolysis[25] and especially Ir−ReOx/SiO_2 was active and selective toward glycerol hydrogenolysis[26] and hydrogenation.[27] Interestingly it was reported in ref 26 that Ir is covered by three-dimensional ReOx clusters, and the authors proposed[27] that hydrogenation involves heterolytic dissociation of H_2 into H^+ and H^- at the interface of Ir and ReOx species. ReOx/CNF has also been applied in guaiacol HDO[5] giving cyclohexane as the main product with 66% yield at 300 °C under 50 bar of hydrogen. In fact, a bimetallic ruthenium−rhenium-containing catalyst supported on a multiwalled carbon nanotube was used in eugenol HDO giving propylcyclohexane as the main product at 200 °C in 1 h.[17] In this work Ir−Re/γ-Al_2O_3 catalysts were prepared by two methods, namely, deposition precipitation and impregnation methods to compare the influence of catalyst synthesis procedure. Catalytic performance was compared with Pt−Re/γ-Al_2O_3 as well as with monometallic catalysts. In addition, catalyst regeneration and reuse were also demonstrated.

EXPERIMENTAL SECTION

Chemicals. The following chemicals were acquired from commercial sources and used without any further purification: isoeugenol (cis + trans) (≥98, Fluka), dihydroeugenol (≥99, Sigma-Aldrich), dodecane (≥99%, Alfa Aesar), benzene (≥99%, Sigma-Aldrich), cyclohexane, (99%, Lab Scan), heptane (≥99, Sigma-Aldrich), 2,5-dimethylhexane (99%, Sigma-Aldrich), 2-hexanol (99%, Aldrich), octane (≥99%, Fluka), propylcyclohexane (99%, Aldrich), mesitylene (98%, Sigma-Aldrich), and diethylbenzene ((≥95%, Fluka). Pyridine was used as a probe molecule (Sigma-Aldrich, ≥ 99.5%, a.r.).

The following gases were used: a gas mixture containing methane 1 vol %, ethane 1.03 vol %, propane 0.981 vol %, isobutene 0.983 vol %, butane 0.96 vol % (AGA), hydrogen (AGA, 99.999%) helium (AGA, 99.996%), and argon (AGA, 99.999%).

Synthesis of Metal Catalysts Supported on Alumina. The IrRe/Al_2O_3 catalyst denoted as IRA-1 was prepared by deposition−precipitation of H_2IrCl_6 (0.5 M) with Na_2CO_3 (1 M) followed by reduction with formic acid (80 °C). After separation, the catalyst was washed, dried (110 °C) overnight, and reduced in H_2 at 400 °C during 3 h (temperature ramp 2 °C/min). This was followed by impregnation with $HReO_4$, drying, and reduction at 420 °C during 3 h (with the temperature ramp 2 °C/min).

Synthesis of other IrRe/Al_2O_3 catalysts denoted as IRA-2 and IRA-3 was completed by incipient wetness impregnation. First, alumina was impregnated with H_2IrCl_6, dried overnight (110 °C), and calcined at 500 °C during 4 h. Then, this sample was split into two parts. One portion was reduced at 450 °C (with the temperature ramping rate of 2 °C/min) during 3 h, then impregnated with $HReO_4$, dried, and reduced similarly to the other portion. This sample was denoted as IRA-2. The other portion was immediately impregnated with $HReO_4$, dried, and reduced at 417 °C during 3 h. This sample was denoted as IRA-3. Monometallic catalysts, Pt/Al_2O_3, Ir/Al_2O_3, and Re/Al_2O_3 denoted as PA, IA, and RA, respectively, were prepared by impregnation of alumina with an aqueous solution of the corresponding metal precursors as described elsewhere,[29] H_2PtCl_6 (0.1 M), H_2IrCl_6 (0.5 M), and $HReO_4$ (1 M), respectively. After impregnation, the samples were dried overnight (17 h, 110 °C) and reduced increasing temperature to 400 °C (Pt/Al_2O_3), 420 °C (Ir/Al_2O_3), and 400 °C (Re/Al_2O_3) with temperature ramping 2 °C/min during 3 h. A bimetallic 3 wt % Pt-3 wt % Re−Al_2O_3 (PRA) with the numbers corresponding to nominal metal loading was prepared by the subsequent impregnation synthesis method of Al_2O_3 with $HReO_4$ and H_2PtCl_6. After impregnating Al_2O_3 with $HReO_4$, the sample was dried at 110 °C for 17 h; thereafter, it was impregnated with H_2PtCl_6 followed by drying at 110 °C for 17 h. The dried mixture containing rhenium and platinum was reduced at 400 °C for 3 h with the temperature ramp 2 °C/min.

Reduction of Catalyst. One day prior to an experiment on HDO of isoeugenol, the fresh catalysts were reduced with hydrogen. First, 50 mg of the catalyst was flushed with argon for 10 min and then with hydrogen for 10 min. The program was set to heat from room temperature to 350 °C in 33 min (with the temperature ramp of 10 °C/min) and keep at 350 °C for 3 h under hydrogen flow. Afterward, as the program was completed and temperature decreased to 100 °C, the catalyst was flushed with argon for 10 min. The solvent (10 mL of dodecane) was added onto the catalyst and kept overnight.

Regeneration of Spent Catalyst. Reproducibility tests were performed for two catalysts such as IRA-1 and IRA-3. After isoeugenol HDO at 250 °C and 30 bar, the spent catalyst was washed with acetone and dried in air. Then, it was calcined under air according to the following program: 25−150 °C at 2 °C/min (40 min); 150−400 °C at 3.3 °C/min (180 min); 400−25 °C at 3.8 °C/min for the regeneration.

Reactor Setup and Analysis. HDO of isoeugenol was performed using a 300 mL stainless steel batch reactor (PARR Instruments) equipped with an axial mechanical stirrer. During experiments, samples were periodically taken. The temperature was kept within ±1 °C, as the reactor was equipped with an automatic temperature control system. The stirring speed was 900 rpm to overcome external mass transfer limitations. The size of catalyst particles was below 63 μm to ensure absence of internal mass transfer limitations. Typically, for HDO of isoeugenol, 50 mg of the catalyst, 100 mg of the reactant, and 50 mL of dodecane were used. The liquid and gas samples taken during the experiments were analyzed by GC and GC/MS. In GC analysis, a DB-1 capillary column (Agilent 122-103e) of 30 m length, 250 μm internal diameter and 0.5 μm film thickness was utilized. Helium was applied as a carrier gas with the flow rate of 1.7 mL/min. The temperature program for GC analysis was as follows: 60 °C (5 min), 3 °C/min to 135 °C, and 15 °C/min to 300 °C. GC-MS analysis was performed over the same column as used in GC. The program applied for the gas analysis was 40 or 60 °C (5 min), 3 °C/min to 135 °C, and 15 °C/min to 300 °C (30 min).

Catalyst Characterization Methods. The majority of characterization methods described below unless specifically mentioned were done for the reduced catalysts. Nitrogen physisorption was performed at 77 K using a Carlo Erba Sorptomatic 1900 device, and a BET program was applied to identify the specific surface area and pore volume of the alumina supported catalysts. The investigated catalysts were heated at 150 °C and outgassed at a pressure lower than 8 mbar for 3 h.

Scanning electron microscopy (SEM) coupled with an energy dispersive X-ray analyzer (EDXA) was utilized to obtain information on the morphology and elemental analysis of the fresh and spent catalysts. A Zeiss Leo Gemini 1530 microscope combined with secondary electron and backscattered electron detectors was applied. An acceleration voltage of 15 kV was used for the X-ray analyzer. In order to perform the analysis, the catalyst was placed as a thin layer on top of the carbon coating to enhance conductivity allowing for a high quality of magnified images.

X-ray diffraction (XRD) reflexes of catalysts were recorded with an X-ray diffractometer D8 (Bruker, Germany) using Cu K radiation and a LynxEye detector by scanning with a step of 0.05° and an accumulation time of 3 s at each point with a slit width 0.26° or accumulation time of 1 s at each point with a slit width of 0.52°.

Transmission electron microscopy (TEM) was utilized to study the morphology and metal particle size. The equipment used for analysis was a JEM-1400Plus (JEOL, Japan) with 120 kV maximal acceleration voltage. The interpretation of TEM images and determination of particles sizes of fresh and spent catalyst were done using the ImageJ program.

DOI: 10.1021/acssuschemeng.8b03035
ACS Sustainable Chem. Eng. 2018, 6, 16205−16218

In addition, high resolution TEM (HRTEM) was performed for IRA-1, 2, 3 on a JEM-2010 microscope (JEOL, Japan) with a lattice resolution of 0.14 nm at an accelerating voltage of 200 kV. Prior to the TEM study, the sample was ground and suspended in ethanol. A drop of suspension was mounted on a copper grid coated with a holey carbon film, and the solvent was allowed to evaporate. The mean size of metal particles for each catalyst was determined by measuring the diameter (d_i) of more than 350 particles seen in TEM micrographs with a medium magnification (e.g., 150,000−200,000 for the particle size 3 nm).

Temperature-programmed reduction with H_2 (TPR) with preliminary reduced catalysts (see catalyst preparation) after a certain storage period was performed in an AutoChem 2910 instrument to explore their on-shelf stability. About 100 mg of catalyst was dried at 120 °C for 1 h followed by reduction with 5 vol % hydrogen in argon using the following temperature program: 25−700 °C at 10 °C/min. A TC detector was used, and a cooling system containing liquid nitrogen, a 2-propanol mixture, was applied to dry gas phase samples before entering the TC detector.

Acidity of the catalysts was determined using pyridine adsorption desorption (ATI Mattson) FTIR. A sample was pressed into a thin pellet with a weight in the range between 10 and 20 mg. The prepared pellet was placed in the cell of a spectrometer for 1 h outgassing in vacuum at 450 °C. Afterward, the sample was cooled to the set temperature of 100 °C, followed by adsorption of pyridine on the pellet surface for 30 min and then recording the scanned spectra. Subsequently, to obtain the acidity strength distribution such as weak, medium, and strong Brønsted and Lewis acid sites, thermal desorption of pyridine was performed at 250, 350, and 450 °C, respectively. The spectral bands integrated at 1455 and 1545 cm^{-1} provided information on the Brønsted and Lewis acid sites concentrations using the extinction coefficients from Emeis.[28]

A ThermoFisher Scientific Flash 2000−combustion CHNS/O analyzer was used to determine the concentration of carbon, hydrogen, nitrogen, and sulfur in the fresh and spent catalysts.

Thermogravimetric analyses (TGA) of the fresh and spent catalysts were carried out using SDT Q600 (V20.9 Build 20) device. Depending on the support, the gas atmosphere was chosen; e.g., air and nitrogen were utilized for the catalysts with alumina as a support, while only nitrogen was used for zirconia and carbon supports. Around 7 mg of catalyst was placed on an alumina sample pan as well as on an empty pan as a reference and heated from room temperature to 1000 °C (temperature ramp of 10 °C/min). The volumetric flow rate used during analysis was 100 mL/min.

Coke was extracted from the spent catalyst using heptane as a solvent.[30] The spent catalyst of 10−20 mg was placed in a round-bottomed boiling flask of 25 mL with a magnetic stirrer and a reflux cooler. Afterward, 20 mL of heptane was added to the flask. Extraction of the spent catalyst was performed for 4 h at 125 °C, which is higher than the boiling point of heptane (98.4 °C). The stirring speed was 375 rpm. After filtration, the spent catalyst was dried under nitrogen flow at 40 °C. Thereafter, the organic residue was dissolved in 10 mL tetrahydrofuran to obtain organic material of around 2 mg/mL. Prior to the size exclusion chromatography (SEC) analysis, the samples were filtered with a membrane PTFE (0.2 mm Teflon filter). SEC-HPLC was equipped with two columns of Jordi Gel DVB 500A (300 mm × 7.8 mm) and a Guard column (50 mm × 7.8 mm). The flow rate was 0.8 mL/min. The column temperature was 40 °C, and the air pressure was 3.5 bar. Because some monomers can be evaporated, the analysis is not fully quantitative.

X-ray photoelectron spectroscopy (XPS) measurements were performed with a PerkinElmer PHI 5400 spectrometer with Mg Kα. The source X-ray was operated at 14 kV and 200 W. The pass energy of the analyzer was 35.45 eV, and the energy step was 0.1 eV. The fitting of the peak was performed using the XPS Peak 4.1 program, and the correction of the background was done applying the Shirley function. The sensitivity factors applied in the quantitative analysis of Al 2p, O 1s, Re 4f, and Ir 4f were 0.234, 0.711, 3.961, and 5.021, respectively. Al 2p (74.4 eV) was utilized as the reference to account for possible charging.

Definitions. The GC based sum of the reactants and products in the liquid phase analysis (GCLPA) was calculated as follows:

$$\mathrm{GCLPA} = \frac{\mathrm{GCLPA}_t}{\mathrm{GCLPA}_0} \times 100\% \quad (1)$$

where, $GCLPA_0$ is the initial GC based sum of the reactants and products in the liquid phase analysis; $GCLPA_t$ is GC based sum of the reactants and products in the liquid phase analysis at time t. This approach was used to evaluate the mass balance in the liquid phase. The rest of the compounds which could not be detected in the liquid phase are either nonvolatile liquid products not eluting from GC, gas phase products, and heavy compounds adsorbed on the catalyst.

Conversion of the reactant was calculated using the following equation:

$$X_{a,t} = \frac{C_0 - C_{a,t}}{C_0} \times 100\% \quad (2)$$

where, $X_{a,t}$ is the conversion at time t, %; $C_{a,0}$ is the initial molar concentration of the reactant, mol/L; $C_{a,t}$ is the molar concentration of the reactant at time t, mol/L.

The yield of propylcyclohexane was calculated by dividing the amount of formed propylcyclohexane after 240 min by the initial amount of isoeugenol.

RESULTS AND DISCUSSION

Characterization of Catalysts. *XRD.* XRD results of IRA and PRA catalysts are shown in Table 2 and Figure 2. The Ir particle size was the smallest for IRA-1 according to XRD, whereas very large particles, about 19 nm, were visible in IRA-2. The Ir particles in IRA-3 were 6.2 nm (Table 2). On the other hand, Re particle sizes were the same, being in the range of 5.3−7.2 nm. It should be noted here that small catalyst particles relevant for catalysis certainly cannot be detected by XRD. The Ir nominal loading was in the range of 3 wt %, while it varied in the range from 0.82 to 3.75 wt % by EDXA (see below). In IRA-1, also an amorphous phase which cannot be directly assigned to any of the metals, was present at 2θ 20°, indicating that its crystallinity is lower than for other catalysts. Different reflexes related to Ir(111), Ir(200), and Ir(311) are clearly visible at 40°, 47°, and 83°, respectively, according to Gutsche et al.[31] and Lejaeghere et al.[32] Reflexes related to Re(100), Re(002), and Re(101) can be seen at 37°, 39°, and 43°, respectively.[33] In IRA-3, part of Re was in the oxidation state as ReO_2 because a 2θ peak at 26 ° was found, while it was not detected for other IRA and PRA catalysts.[34]

Table 2. Metal and Metal Oxide Particle Size and Phase Composition Determined by XRD

Catalyst	Ir (wt %)	Re (wt %)[a]	Ir particle size (nm)	Re particle size (nm)
IRA-1	3.1	1.1	2.0	7.2
IRA-2	3.5	4.4	19.0	5.3
IRA-3	2.9	4.6 (2.4)	6.2	6.2
PRA	1.3[b]	0[c]	6.5[b]	0

[a]In parentheses, ReO_2 wt %. [b]Pt. [c]The rest is alumina.

A part of Re was in the oxidation state as ReO_2 in IRA-2 because a 2θ peak at 26° was found, while it was not detected for other IRA and PRA catalysts.[34] The Pt particle size in the PRA catalyst was 6.2 nm. Pt diffraction peaks are also clearly visible being at the same positions as found for Ir.[31] According to XRD, the Al_2O_3 phase in the pristine support and the

DOI: 10.1021/acssuschemeng.8b03035
ACS Sustainable Chem. Eng. 2018, 6, 16205−16218

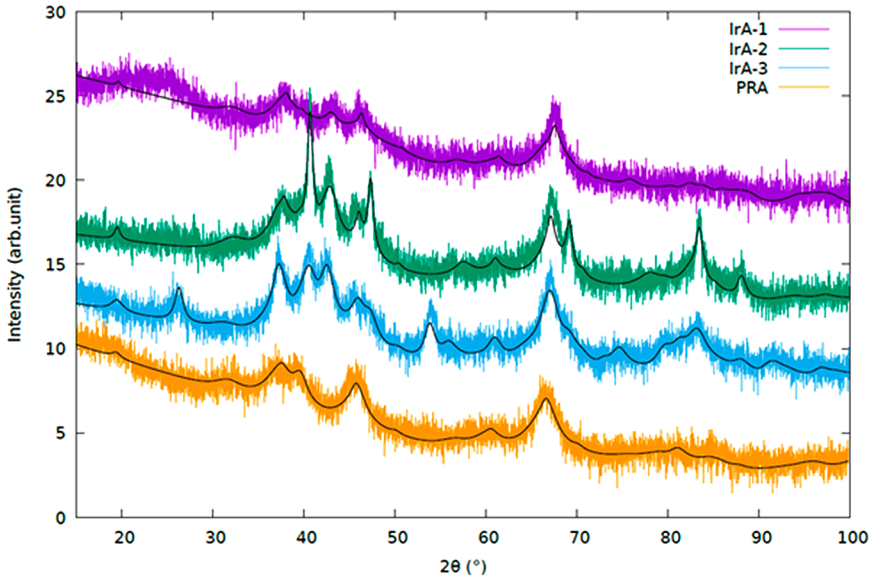

Figure 2. XRD results from different catalysts.

catalysts was γ-alumina without any reflexes related to boehmite.[35]

Textural Properties. The specific surface area among the studied catalysts was the highest for PRA being 243 m^2/g (Table 3), while the lowest one was measured for IRA-1 prepared via the deposition−precipitation method. It can also be noted that the specific surface areas of IA and IRA-1 are lower than for RA, IRA-2, and IRA-3, indicating some pore blockage in IA and IRA-1. Noteworthy is also that IA and RA are prepared both with the impregnation method using an aqueous slurry. IRA-1 exhibiting smaller specific surface area is prepared by the deposition−precipitation method, whereas IRA-2-and IRA-3 were synthesized by the incipient wetness method. As a comparison, it can be noted that the commercial mesoporous alumina support used for the catalyst preparation has a specific surface area of 250 m^2/g, which is the closest to PRA.[35]

Table 3. Metal Particle Size and Specific Surface Areas of Tested Catalysts

Catalyst	Metal particle size in fresh catalyst (nm) (metal dispersion (%))	Metal particle size in spent catalyst (nm)	Specific surface area (m^2/g_{cat})[a]	Pore volume (cm^3/g_{cat})[a]
IA	n.d.[b]	n.d.	101	0.21
RA	5.3 (19)	5.3	150	0.53
PA	10.3 (10)	4.9	n.d.	n.d.
PRA	3.4 (29)	2.8	243	0.74
IRA-1	0.9[c] (100)	1.9	101 (101)	0.20 (0.19)
IRA-2	0.9[c] (100)	1.4	216	0.76
IRA-3	0.7[c] (100)	0.7	215 (203)	0.70 (0.72)

[a]Spent catalyst in parentheses. [b]n.d. not determined. [c]HR-TEM

SEM. SEM images of PA, RA, and PRA are shown in Figure S1. The catalyst particle size of PA varies in the range from 25 to 180 μm with no large differences visible in the fresh and spent catalysts (Figure S1a and b). Fresh RA exhibited a smooth surface covered by small particles not visible in the spent RA (Figure S1c and d). For PRA, the fresh and spent catalysts resembled each other (Figure S1e and f), both exhibiting irregular particles in the range between 1 and 5 μm.

SEM images revealed (Figure S2) that the morphologies of impregnated IRA-2 and IRA-3 catalysts are different from IRA-1, prepared by the deposition−precipitation method. The shape of IRA-1 particles was poorly defined, while IRA-2 and IRA-3 exhibited mainly spherical and some oval shapes (34−210 μm). In addition, the two latter ones have a significant amount of needle-shaped particles containing iridium according to EDX analysis. SEM-EDX analysis confirmed the presence of needle shaped agglomerates (stars) which belong to iridium metal particles (Figure S2c).

Based on SEM-EDX analysis, the Re/Ir weight ratio decreased as follows for the fresh IRA catalysts: IRA-1 > IRA-3 > IRA-2 being respectively 4.4, 2.6, and 1.4 (Table 4).

Table 4. EDXA Analysis Results of Fresh and Spent IRA Catalysts[a]

	PRA		IRA-1		IRA-2		IRA-3	
Ratio	Fresh	Spent	Fresh	Spent	Fresh	Spent	Fresh	Spent
Pt	2.8		–	–	–	–	–	–
Re/Pt	1.3	1.1	–	–	–	–	–	–
C/Pt	5.1	4.6	–	–	–	–	–	
Ir	–	–	0.82	0.74	3.75	1.65	1.74	1.97
Re	3.7	–	3.46	4.16	5.37	2.99	4.6	3.52
Re/Ir	–	–	4.4	5.6	1.4	1.8	2.6	1.8
C/Ir	–	–	21	21	3	10.8	8.2	8.4

[a]The catalysts have been used in isoeugenol HDO at 250 °C under 30 bar total pressure. The values are given in wt % of each element.

The largest deviation in the Re/Ir ratio in comparison with XRD results (Table 2) is in IRA-1 for which this ratio was only 0.35. For IRA-2 and IRA-3, the Re/Ir ratio was comparable. Furthermore, for the spent catalysts, the carbon to metal weight ratio was determined showing that especially IRA-2 exhibited extensive coking, as its C/Ir ratio increased. It should be noted that in the SEM-EDX analysis there is also a contribution of carbon coming from a carbon coating placed below the catalyst layer. The presence of hydrogen also

DOI: 10.1021/acssuschemeng.8b03035
ACS Sustainable Chem. Eng. 2018, 6, 16205−16218

indicates the presence of hydrocarbons on the spent IRA-2. The CHNS analysis showed also a high amount of carbon in this catalyst (see below).

TEM. TEM images of PRA catalysts showed that metal particles were about 3.4 nm, and no sintering occurred when this catalyst was used in HDO of isoeugenol at 250 °C under 30 bar (Figure S3). TEM images of RA and PA are shown in Figure S4a and b. Interestingly, monometallic catalysts contain particles with a size larger than in bimetallic PRA. IRA catalysts and the metal particle size distribution revealed that despite different synthesis methods IRA-1 and IRA-2 exhibited the same metal particle sizes in the fresh catalysts, i.e., 0.9 nm analyzed by high resolution transmission electron microscopy (HR-TEM) (Table 3, Figure S5). On the other hand, slightly smaller metal particles (0.7 nm) were found in IRA-3, prepared via consecutive impregnation of Ir and Re precursors, while slightly larger metal particles (0.9 nm) were present in IRA-2, in which the alumina-supported Ir precursor was reduced prior to impregnation of $HReO_4$.

In addition, the spent catalysts, used in HDO of isoeugenol, were also investigated by TEM. The results showed that iridium metal particle sizes varied in the range of 0.7−1.9 nm (Table 3). The size range of metal particles in spent IRA-1 increased slightly due to the appearance of agglomerates in the spent catalyst. It should, however, be noted that it is difficult to directly compare the metal particle sizes for the fresh and spent catalysts since different TEM equipment was used. Extensive sintering of the metal particles, is, however, not probable due to a rather low HDO temperature. TEM images of spent IRA-2 and IRA-3, however, revealed the presence of some needle-shaped large agglomerates (visible even by SEM) with the size varying from ca. 150 to 1100 nm in the fresh and spent catalysts. This type of agglomeration was not detected for IRA-1.

TPR. Temperature-programmed reduction made for the preliminary reduced catalysts (Figure 3) revealed substantial amounts of hydrogen consumed by the catalysts after storage. Hydrogen quantities in the reduction of different catalysts decreased in the following relative order calculated per mass of metal (determined by EDXA (Table 4)) with the corresponding values: PRA (36.9) > IRA-3 (25.2) ≥ IRA-1 (23.4) ≫ IRA-2 (11.0). It can be seen that IRA-1 and IRA-3 exhibited nearly the same amounts of hydrogen consumed, whereas IRA-2 was less than half of their values. Amounts of hydrogen consumed for PRA were slightly higher than IRA-3 with about the same metal loading. It should, however, be pointed out that the Re/Pt ratio of 1.3 was lower in PRA compared to the Re/Ir ratio in IRA-3 of 2.6, indicating that Ir and Pt are more easily reduced than ReOx, and their amounts can be correlated with TPR. In IRA-1, the largest peak for hydrogen consumption was obtained at 220 °C, whereas only a small peak was present at 370 °C. The hydrogen consumption at 220 °C is close to the one reported in ref 36 for reduction of $IrCl_3$ supported on Al_2O_3 at 230 °C. Reduction of rhenium, however, occurs according to the literature[37] at 447 °C, which is much higher. In IRA-3, the largest hydrogen consumption occurred at 255 °C, whereas also a relatively large amount of hydrogen was consumed at 470 and 500 °C. The two latter peaks are more close to reduction of rhenium oxide reported in the literature. IRA-2 exhibited the lowest hydrogen uptake with the first peak occurring at 270 °C and a small one at 470 °C. PRA exhibits the highest hydrogen consumption at 220 °C, which is close to the reduction temperature for well dispersed Pt[38] at 213 °C. In addition, PRA exhibited two more peaks consuming hydrogen at 380 and 465 °C, respectively. It has been reported in ref 38 that a second peak consuming hydrogen for Pt/Al_2O_3 can originate from reduction of $Pt(OAl)_4$ at 414 °C. On the other hand, the PRA catalyst exhibiting a Re/Pt mass ratio of 1.3 was dried at 110 °C, after which it was reduced at 400 °C. For the $Pt–Re/Al_2O_3$ catalyst with a Re/Pt ratio higher than 0.6, it was concluded that Re is not completely reduced.[39] Only a part of Re^{7+} has been reduced to metallic Re. A possible alloy formation is difficult to assess only by TPR. It has been stated in ref 39 that Re in Re/Al_2O_3 was reduced at 400−450 °C.[40] The peak at 465 °C is close to the one reported for reduction of rhenium.[37] Overall, it can be concluded that catalyst reduction prior to experiments is essential as the catalysts underwent at least partial oxidation during storage.

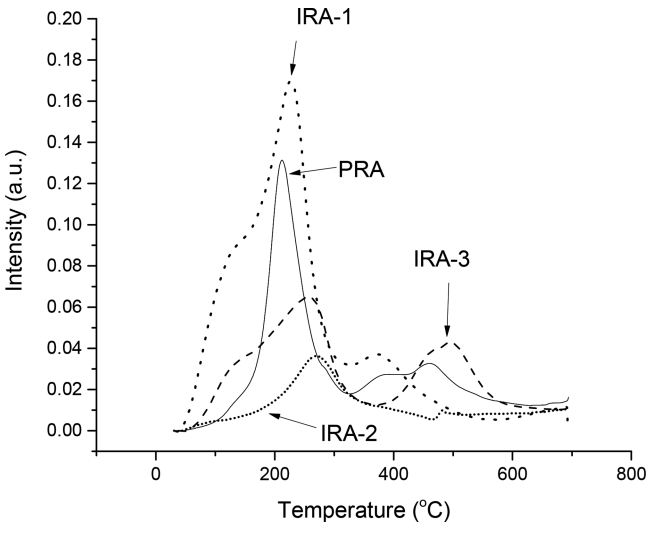

Figure 3. TPR of IRA and PRA catalysts.

XPS. The XPS results from IRA-1, IRA-2, and IRA-3 catalysts showed that iridium was present with the binding energies of 61.7, 61.2, and 62.1 eV for the fresh IRA series catalysts, respectively, corresponding to the valence state of 4+ (Figure 4a). For the spent IRA-1 and IRA-2 catalysts, the binding energies were increased by 0.2 eV, while for the spent IRA-3 the binding energy was dropped by 0.2 eV (Figure 4b). Therefore, a nonsignificant change occurred for the catalysts after isoeugenol HDO indicating the same valence state of 4+. Based on Freakley et al.,[41] the mean binding energy of 61.9 eV (±0.7) corresponds to IrO_2, while typical binding energies for carbon-supported Ir(IV) are 62.2 eV[42] and Ir(III) 62.0 eV,[43] whereas for metallic iridium (iridium black) the binding energy is 60.7 eV.[42] Comparison of the weight ratio between Re/Ir determined by XPS and EDXA (Table 5) shows that the former method results in a Re/Ir ratio higher than the latter one, indicating some surface enrichment of ReOx species because XPS results correspond to the surface concentration, whereas XRD reflects the bulk analysis. This result is in line with the literature data[27] reporting that ReOx species can cover Ir species.

In addition, the atomic ratios of Ir/Al and Re/Al were calculated for IRA catalysts (Table 5) showing that for IRA-1 the Re/Al ratio was the highest followed by IRA-3. The presence of different rhenium valence states was found in IRA series catalysts, with the major valence state being 7+. Rhenium 7+ corresponds to the binding energy between

DOI: 10.1021/acssuschemeng.8b03035
ACS Sustainable Chem. Eng. 2018, 6, 16205−16218

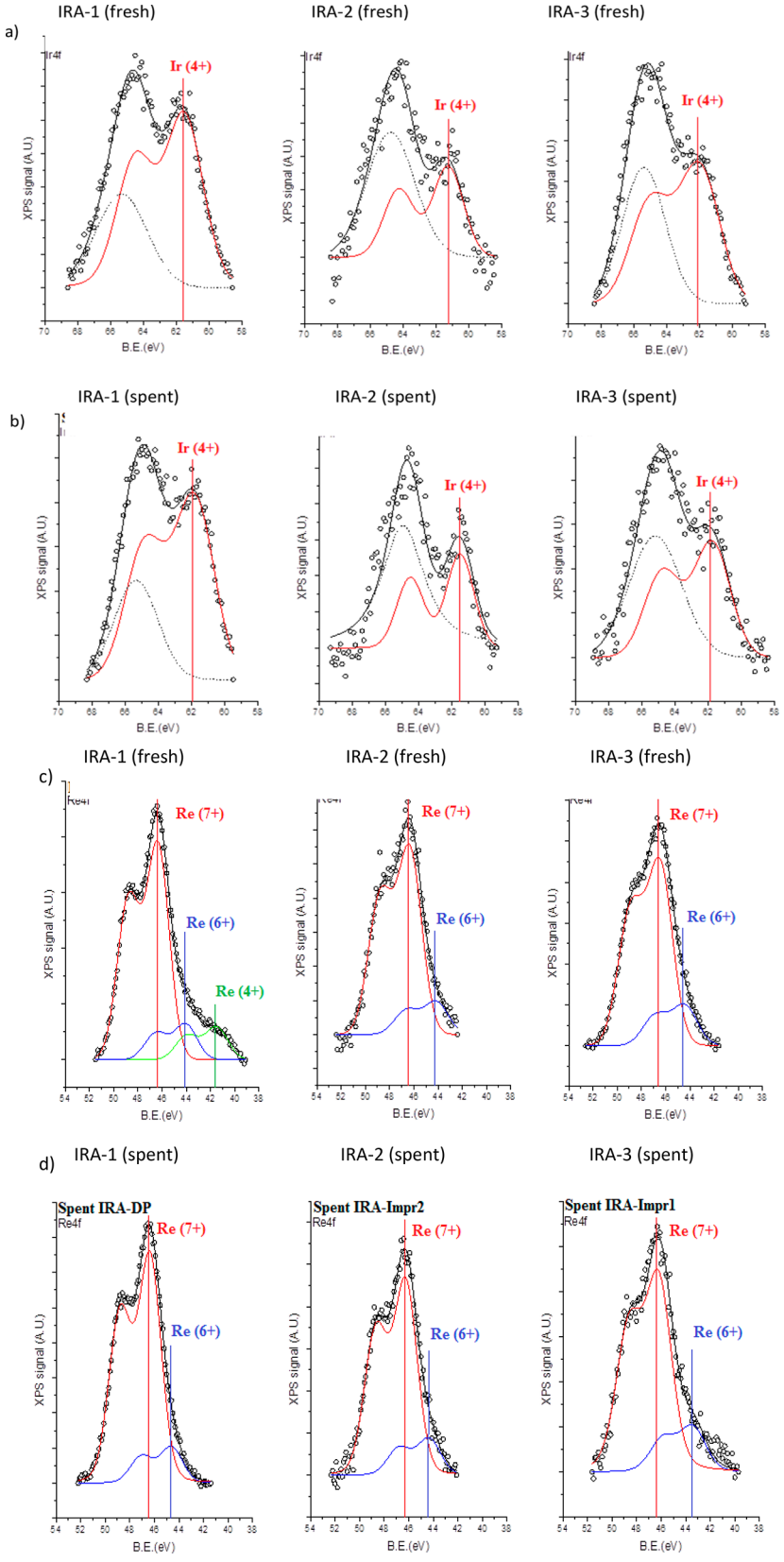

Figure 4. XPS results indicating iridium valence state for the (a) fresh and (b) spent and rhenium valence state for the (c) fresh and (d) spent IRA series catalysts obtained after isoeugenol HDO at 250 °C and 30 bar.

45.4 and 46.9 eV in both fresh and spent catalysts according to Shpiro et al.[44] The valence state 6+ in the range between 44.2 and 44.8 eV was also present in the fresh and spent catalysts except for the spent IRA-3. The fresh IRA-1 catalyst exhibited not only 7+ and 6+ valence states but also a 4+ state at the binding energy of 41.8 eV (Figure 4c, d), similar to

DOI: 10.1021/acssuschemeng.8b03035
ACS Sustainable Chem. Eng. 2018, 6, 16205−16218

Table 5. XPS Results from Fresh and Spent IRA Catalysts

Catalyst	Al 2p (wt %)	O 1s (wt %)	Re 4f (wt %)	Ir 4f (wt %)	Re^{7+} (%)	Re^{6+} (%)	Re^{4+}(%)	Ir/Al Atomic ratio	Re/Al Atomic ratio
IRA-1-fresh	31.0	43.7	20.9	4.4	75.8	12.7	11.5	0.02	0.10
IRA-1-spent	33.5	43.7	18.9	3.9	86.3	13.7	0	0.02	0.008
IRA-2-fresh	43.0	46.2	9.3	1.5	85.0	15.0	0	0.006	0.03
IRA-2-spent	41.7	47.8	9.1	1.5	84.0	16.0	0	0.006	0.03
IRA-3-fresh	40.3	47.8	9.6	2.3	81.8	18.2	0	0.009	0.03
IRA-3-spent	36.9	52.3	9.1	1.8	81.0	19.0	0	0.007	0.03

Rozmysłowicz et al.[45] However, the valence state 4+ for rhenium was absent in the spent IRA-1 being used in isoeugenol HDO at 250 °C and 30 bar. When comparing the XPS results with XRD results, it can be seen that the XPS results show Re^{4+} in IRA-1 (Figure 3a), but XRD does not detect it in that sample (Figure 2). The difference in XPS and XRD analysis is that the XPS analysis is taken from the catalyst surface, whereas XRD is identifying the bulk composition. In the current case, IRA-1 contains Re^{4+} on its surface determined by XPS, whereas IRA-3 has ReO_2 in the bulk phase, determined by XRD.

TGA. TGA was performed for the fresh catalysts as well as for the spent ones after isoeugenol HDO at 250 °C and 30 bar in order to elucidate the mass balance closure by taking into account coke formation. IRA-3 contained 4.1 wt % coke in TGA performed in nitrogen, while in air the amount of coke was 1.7 wt % (Figure S6b). In air, a notable endothermic peak can be observed around 400 °C due to oxidation of a part of coke.

Organic Elemental Analysis. Organic elemental analysis results showed that the carbon content increases after isoeugenol HDO at 250 °C and 30 bar in the spent IRA catalysts series indicating coke formation (Table 6). Spent

Table 6. CHNS Results for IRA Catalysts

Catalyst	Type	Carbon (% w/w)	Hydrogen (% w/w)	Nitrogen (% w/w)	Sulfur (% w/w)
IRA-1	fresh	0.20	0.49	0.00	0.03
IRA-1	spent	1.60	0.60	0.02	0.00
IRA-2	fresh	0.13	0.79	0.00	0.00
IRA-2	spent	26.50	4.79	0.03	0.00
IRA-3	fresh	0.99	0.78	0.00	0.00
IRA-3	spent	2.80	0.90	0.02	0.00

IRA-1 and IRA-3 exhibited only minor coking, while in the spent IRA-2 there was a significant increase in the carbon content by ca. 26%, which together with its lower hydrogen consumption in TPR can partially explain its low catalytic activity compared to IRA-1 and IRA-3 as discussed below. Note that despite a much higher level of carbon content observed in IRA-2 IRA catalysts were characterized by only a minor difference in GCLPA, i.e., 45% for IRA-2 vs 53% for IRA-1 and 54% for IRA-3.

Pyridine adsorption−desorption results showed that the majority of the catalysts exhibited weak acid sites, and the amounts of medium and strong Brønsted acid sites were very small in IRA-2 and IRA-3 (Table 7). Only PRA exhibited a very small amount of strong sites desorbing above 450 °C.

Isoeugenol Hydrodeoxygenation. Isoeugenol transformation at 250 °C under 30 bar total pressure in hydrogen resulted in rapid hydrogenation of isoeugenol even in the absence of any catalyst (Table 8, entry 1), analogously to the results obtained by Bjelik et al.[13]

Table 7. Amount of Brønsted and Lewis Acid Sites Determined by FTIR Pyridine Adsorption Desorption Method

	Brønsted acid sites (μmol/g_{cat})			Lewis acid sites (μmol/g_{cat})		
Catalyst	250 °C	350 °C	450 °C	250 °C	350 °C	450 °C
IA	n.d	n.d	n.d	n.d	n.d	n.d
RA	n.d.	n.d.	n.d.	n.d.	n.d.	n.d.
PA	16	0	0	88	4	1
PRA	16	0	0	88	4	1
IRA-1	19	0	0	0	0	0
IRA-2	10	1	0	109	9	0
IRA-3	1	1	1	106	1	0

In catalytic HDO of isoeugenol, both mono- and bimetallic Pt-, Ir-, and Re-modified catalysts were investigated. Since isoeugenol hydrogenation was typically very rapid, initial TOF of the transformation of dihydroeugenol was calculated between 1 and 30 min by dividing the moles of converted dihydroeugenol by time and moles of the surface metals determined by EDXA (eq 3). The amount of surface metals is obtained by dividing the sum of metal masses (Ir, Re) determined from EDXA by metal dispersion.

$$\mathrm{TOF} = \frac{(n_{\mathrm{DH2}} - n_{\mathrm{DH1}})}{\triangle t n_{\mathrm{Metal}}} \quad (3)$$

The initial TOF values over IA, RA, and IRA-1 catalysts in HDO of isoeugenol at 200 °C were very low (Table 8, entries 2, 3, and 7) corresponding to formation of dihydroeugenol as the main product. GCLPA was lower for IA at 200 °C compared to the RA and IRA-1. The yield of dihydroeugenol after 240 min decreased in the following order: IRA-1 > IA > RA. Noteworthy is that despite a low specific surface area of IRA-1 it exhibited a high metal dispersion (Table 3), and it could produce a high yield of dihydroeugenol (Table 8).

A comparative study of PA, RA, and PRA in isoeugenol HDO at a higher temperature (250 °C) under 30 bar total pressure showed that PA was more active in transforming isoeugenol compared to RA and PRA (Table 8, entries 4−6, Figure 5). On the other hand, conversion of dihydroeugenol was the highest with PRA after 240 min followed by RA and PA (Figure 5a). For PA, the propylcyclohexane yield is only 2.5% yield, and dihydroeugenol is main product 72% yield. The GCPLA decreased in the same order for these catalysts. No propylcyclohexane was formed in eugenol HDO in the case of a monometallic Pt/Al_2O_3 catalyst[11] at conditions similar to the current work, while the PA catalyst utilized in this study was able to produce small amounts of propylcyclohexane due to the absence of Re (Table 7). Furthermore, it was reported by Ghampson et al.[5] that ReOx/CNF was active in HDO of different phenolic compounds being able to produce hydrocarbons at 300 °C under 50 bar hydrogen. Most probably a

DOI: 10.1021/acssuschemeng.8b03035
ACS Sustainable Chem. Eng. 2018, 6, 16205−16218

Table 8. Results from Isoeugenol Hydrodeoxygenation in Dodecane over Different Catalysts[a]

Entry	Catalyst	Initial isoeugenol concentration (mol/L)/(mass of catalyst) (g)	Reactant to catalyst mass ratio	Temperature (°C)	Pressure (bar)	Initial TOF (1/s)	Conversion of dihydro-eugenol after 60 min (%)	GCLPA after 240 min (%)	Main product	Yield of main product (%) after 240 min
1	No catalyst	0.014	No catalyst	250	30	Low	0	90	dihydroeugenol	93
2	IA	0.013/(0.05)	2	200	30	Low	1	69	dihydroeugenol	69
3	RA	0.013/(0.05)	2	200	30	0	0	89	dihydroeugenol	84
4	RA	0.014/(0.05)	2	250	30	0	0	57	dihydroeugenol	50
5	PA	0.013/(0.05)	2	250	30	0.003	10	76	dihydroeugenol	4
6	PRA	0.013/(0.05)	2	250	30	0.001	85 (180 min)	45	propylcyclohexane	54
7	IRA-1	0.013/(0.05)	2	200	30	0.0006	7	80	dihydroeugenol	75
8	IRA-1	0.013/(0.05)	2	250	30	0.0035	24	53	propylcyclohexane	69
9	IRA-1	0.093/(0.1)	7.6	250	30	0.011	25	52	propylcyclohexane	47
10	IRA-1	0.098/(0.4)	2	250	30	0.004	77	79	propylcyclohexane	57
11	*IRA-1-reg.*	0.013/(0.05)	2	250	30	0.0003	61	62	propylcyclohexane	40
12	IRA-2	0.013/(0.05)	2	200	30	0.0007	9	64	dihydroeugenol	90
13	IRA-2	0.013/(0.05)	2	250	30	0.0012	17	45	propylcyclohexane	46
14	IRA-2	0.013/(0.05)	2	250	30	0.0017	17	50	propylcyclohexane	50
15	IRA-3	0.013/(0.05)	2	250	30	0.003	24	54	propylcyclohexane	46
16	IRA-3	0.014/(0.05)	2	250	17	0.0016	16	63	dihydroeugenol	57
17	IRA-3	0.013/(0.05)	2	250	25	0.003	30	48	propylcyclohexane	50
18	IRA-3	0.015/(0.05)	2	250	40	0.0008	16	84	propylcyclohexane	99

[a]Conditions: total pressure, 30 bar; amount of dodecane 50 mL.

higher reaction temperature is needed for HDO of isoeugenol over rhenium supported on alumina.

Comparison of Different IRA Catalysts. The results on HDO of isoeugenol with bimetallic IRA catalysts are shown in Table 8 (entries 7−17, Figure 6). When comparing the performance of three different IRA catalysts at 250 °C under 30 bar hydrogen, the initial isoeugenol concentration was 0.0012 mol/L (Table 8, entries 8, 13, and 15), and in these experiments, complete conversion of isoeugenol was obtained. The initial TOF values for transformation of dihydroeugenol over IRA catalysts at 250 °C under 30 bar (Table 8, entries 8, 13, 15) showed that TOF decreased as follows: IRA-1 > IRA-3 > IRA-2 in the same order as the declining hydrogen consumption determined by hydrogen TPR. A higher availability of hydrogen on IRA-1 is due to a higher weight ratio of Ir/Re determined by XRD, equal to 2.8, whereas this ratio for IRA-2 and IRA-3 was 0.79 and 0.63, respectively. A high catalytic activity of IRA-1 and IRA-3 can also be partially related to the presence of Re^{4+} species, as described previously in the literature.[5] According to XPS, IRA-3 contained Re^{4+} on its surface, whereas ReO_2 was present according to XRD in IRA-3. It can be also speculated that while ReO_2 is probably a separate phase Re^{4+} could be partly reduced species in close contact with Ir and thus be more active. Reproducibility tests of IRA-2 for HDO of isoeugenol (Table 8, entries 13 and 14, Figure 7) showed satisfactory results.

The main product in isoeugenol HDO at 250 °C under 30 bar over IRA catalysts was propylcyclohexane with the decreasing yield as follows: IRA-1 > IRA-3 ≥ IRA-2 (Table 8, entries 8, 13, 15, Figure 6a). The yield of propylcyclohexane was higher over IRA-1 compared to IRA-2, and at the same time, GCLPA was higher for the former catalyst. Typically only traces of other products such as dihydroeugenol, 3-methylheptane, 1-methyl-2-propylcyclohexane, and propylbenzene were formed. Since Re/Al_2O_3 facilitated the formation of propylcyclohexane at 250 °C under 30 bar (Figure 8), the role of metallic rhenium cannot be excluded in IRA-1, which contained according to XPS the highest atomic ratio of Re/Al (Table 5) among the three IRA catalysts. This result is in agreement with the work of Jung et al.,[17] who performed eugenol HDO over RuRe supported on carbon nanotubes at 200 °C in 1 h in heptane under 20 bar hydrogen with the main product propylcyclohexane with 63% selectivity at 99.4% conversion.[17] It was also stated by the same authors[17] that the valence state of Re is important for a highly active HDO catalyst. The most active RuRe catalyst, RuRe/MWCNT exhibited the highest hydrogen consumption in TPR. Furthermore, this catalyst contained large amounts of Re^{4+} according to XPS.[17]

Since different catalysts exhibited different metal loadings, the concentrations of dihydroeugenol and propylcyclohexane were compared by plotting them vs normalized time (time multiplied by mass of metals in the catalyst with the metal loadings taken from EDXA analysis) (Figure 6). IRA-2 and IRA-3 catalysts exhibited similar kinetic trends, in which dihydroeugenol was initially transformed more slowly compared to IRA-1. Conversion of dihydroeugenol was similar (24%) for IRA-1 and IRA 3 after 60 min, while it was only 17% for IRA-2 (Table 8, entries 8 and 15). At the same time, GCLPA at the same normalized time (time multiplied by mass of metals) was 68% for IRA-2 with an Re/Ir ratio of 1.4 and a low hydrogen consumption according to TPR. For IRA-1 and IRA-3 catalysts, the corresponding values of GCLPA were 53% and 54%, respectively.

Partially low GCLPA values can be explained by formation of gaseous products as discussed below. It should be also noted that even with IRA-3 heavy oligomers (Figure S7) were found on the catalyst surface as confirmed by SEC analysis of the extracted organic material from the spent catalyst. The products found in SEC were the monomer, tetramers, and hexamers of phenolic compounds according to calibration with polystyrene. Furthermore, a large peak in SEC was present

DOI: 10.1021/acssuschemeng.8b03035
ACS Sustainable Chem. Eng. 2018, 6, 16205−16218

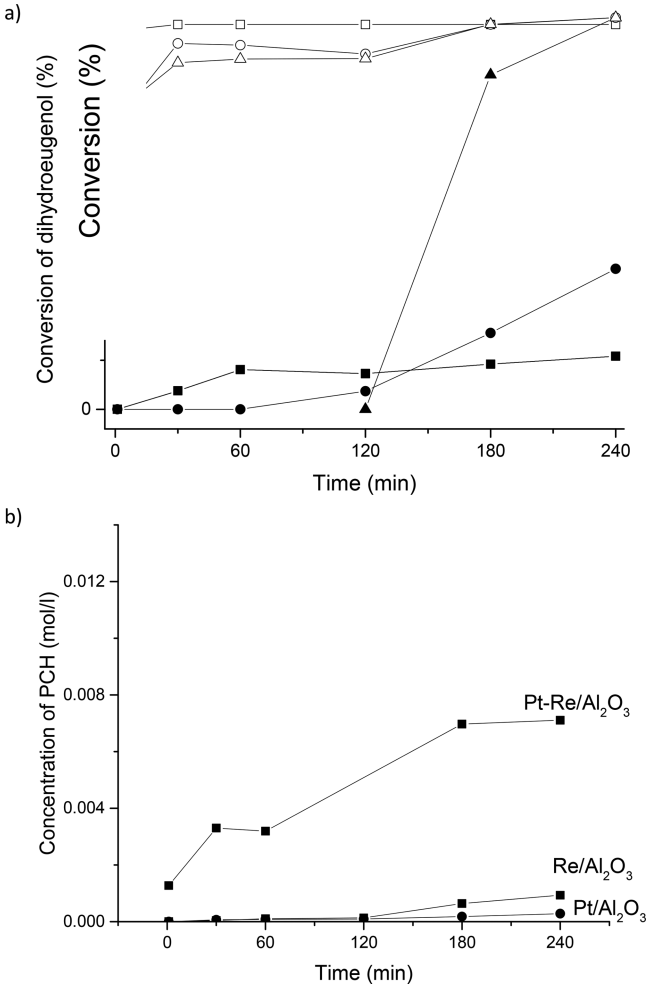

Figure 5. (a) Conversion of isoeugenol (open symbol) and dihydroeugenol (filled symbol) as a function of time and (b) concentration of propylcyclohexane in HDO of isoeugenol over PA (■), RA (●), and PRA (▲) at 250 °C under 30 bar total pressure.

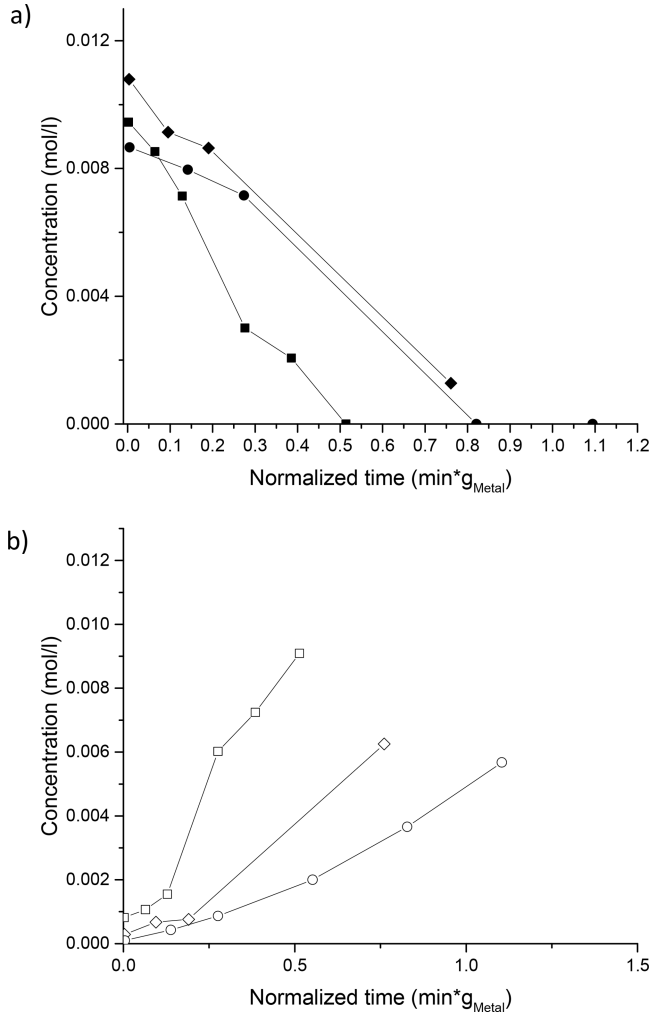

Figure 6. Concentration of (a) dihydroeugenol and (b) propylcyclohexane over IRA-1 (□), IRA-2 (○), and IRA-3 (◊) catalyst as a function of normalized time (time multiplied by mass of metal) in isoeugenol HDO under 30 bar total pressure at 250 °C. Notation: Catalyst amount, 50 mg; initial reactant concentration, 0.013 mol/L.

corresponding to a large molecular weight at retention time of 14.6 min. Because the IRA-1 catalyst was only very mildly acidic (Table 7), acidity was not the origin of a low GCLPA. This catalyst contained, however, well dispersed Ir, which might be a reason for its high hydrogenolysis activity[46] providing low GCLPA. According to XPS analysis, IRA-1 in addition contained also Re^{4+}, which was not present in IRA-3. It is noteworthy, however, that 80% GCLPA was obtained for IRA-3 with a rather high deoxygenation activity. Both IRA-2 and IRA-3 exhibited mainly Lewis acidity, which was absent in IRA-1.

By comparing the concentrations of the formed propylcyclohexane with the ratio of Re to Ir metals obtained via EDX analysis in different IRA catalysts (Table 4), it can be concluded that the higher the weight percentage ratio is between these metals, the higher the concentration of the main product is. IRA-1 exhibited a high weight percentage ratio of Re/Ir of 4.4, while IRA-3 and IRA-2 had 2.7 and 1.4, respectively. According to Liu et.al,[23] the weight ratio of Re to Ir played a significant role in HDO of furylmethane forming alkanes (>82%) for the aviation jet fuel, with the Re/Ir ratio of 2 giving the best results.

The gas phase analysis results from isoeugenol HDO at 250 °C under 30 bar using IRA-1 and IRA-3 confirmed the presence of high amounts of methane and especially ethane followed by propane. It should be noted that the quantity of propane was higher in the presence of IRA-3 compared with IRA-1. In addition butane was also found by GC-MS (Figure S8). Hexane, heptane, and octane were present in both gaseous samples using IRA-1 and IRA-3. Moreover, the main reaction product propylcyclohexane was also present in the gas phase. These data are supported by a known ability of Ir/γ-Al_2O_3 to catalyze hydrogenolysis of cyclohexane at 260 °C in the gas phase.[46] When comparing the current results with the gas phase composition obtained in HDO of eugenol over Ru/C,[13] it can be seen that methane and C9−C13 hydrocarbons were also observed by Bjelic et al.[13] Thus, selection of the metal is crucial for formation of C4 to C6 hydrocarbons observed in the current work.

In addition to formation of the liquid and gaseous products, also solid organic carbon was formed on the surface of the spent catalysts, which was investigated by EDX and OEC methods. When comparing the EDX results of the fresh and spent IRA-1 and IRA-3 (Table 4), it can be seen that the weight ratio of Re/Ir and C/Ir did not significantly change indicating that coking of the catalyst was not very extensive.

DOI: 10.1021/acssuschemeng.8b03035
ACS Sustainable Chem. Eng. 2018, 6, 16205−16218

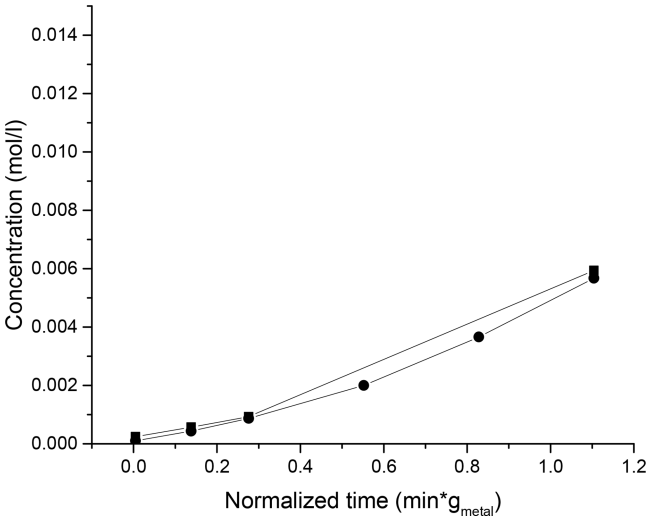

Figure 7. Reproducibility test for isoeugenol HDO over IRA-2 under 30 bar at 250 °C using the isoeugenol initial concentration of 0.013 mol/L, 50 mg of catalyst, and 50 mL of dodecane. Notation: concentration of the formed propylcyclohexane in experiment 1 (○) and 2 (□).

For IRA-2, however, an extensive carbon accumulation was observed both by EDX and OEC analyses indicating possible hydrocarbon deposition blocking access to the catalytically active sites.

Effect of Initial Isoeugenol Concentration. The effect of the initial reactant concentration was investigated using 0.013, 0.093, and 0.098 mol/L initial isoeugenol concentrations, respectively, over IRA-1 as a catalyst in isoeugenol HDO at 250 °C under 30 bar (Table 8, entries 8−10, Figure 8a). The results revealed that the 9.3-fold enhancement of TOF was obtained in the initial TOF of dihydroeugenol with an increase in the initial isoeugenol concentration. The concentration of dihydroeugenol is plotted in Figure 8b as a function of normalized time because of different catalyst to reactant ratio. It can be concluded that the normalized rate for dihydroeugenol transformation increased substantially for a higher initial isoeugenol concentration indicating that the reaction order with respect to the reactant is about unity at low IE initial concentration but tend to a zero at higher initial concentrations.

Formation of propylcyclohexane was lower when using a higher reactant to catalyst ratio in isoeugenol HDO at 250 °C and 30 bar over IRA-1 (Table 8, entry 9). With a lower initial isoeugenol concentration of 0.013 mol/L and with the reactant to catalyst weight ratio of two the yield of propylcyclohexane was 69% (Table 8, entry 8).

Effect of Pressure. The effect of hydrogen pressure in the range of 17−40 bar was also investigated using IRA-3 catalyst (Table 8, entries 15−18, Figure 9). There was a clear retardation of HDO at the lowest pressure value of 17 bar, while higher total pressures prevented catalyst deactivation. After prolonged reaction times, dihydroeugenol was completely converted at higher pressures, while a part of dihydroeugenol was still present at 25 bar even after 240 min.

Dihydroeugenol was the main product at a lower pressure over IRA-3 and GCLPA was also higher under these conditions (Table 8, entry 16). GCLPA increased from 40% to 45% at 25 and 30 bar to 84% when the total pressure of 40 bar was applied. This result is in accordance with Jongerius et

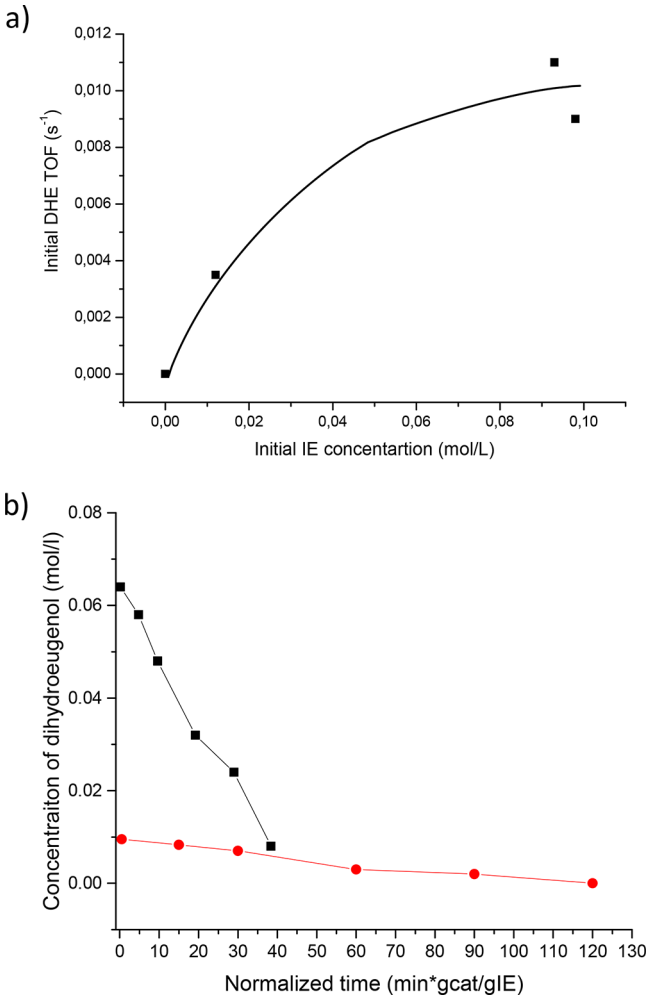

Figure 8. Effect of initial concentration of isoeugenol on HDO over IRA-1 catalyst. (a) Initial TOF of dihydroeugenol as a function of initial isoeugenol concentration. (b) Concentration of dihydroeugenol vs normalized time in HDO of isoeugenol. Notation: (■) 0.1 g of IRA-1 catalyst and 0.62 g of isoeugenol; (●) 0.05 g of IRA-1 catalyst and 0.1 g of isoeugenol. Conditions: 30 bar total pressure at 250 °C in dodecane.

al.,[47] who investigated guaiacol HDO over Mo_2C and W_2C supported on CNF catalyst. In the current work, the highest propylcyclohexane yield was obtained at 40 bar (Table 8, entry 18, Figure 9b). The effect of pressure in eugenol HDO has been scarcely investigated.[13,20] Direct comparison of the pressure effect in the current work and in the literature is not straightforward because the Ru/C catalyst was used in ref 13 in the temperature and pressure ranges of at 275 °C and 40−70 bar. The main product on Ru/C was 2-methoxypropylcyclohexanol due to a low acidity of Ru/C catalyst.[13] Effect of the pressure on further transformations of dihydroeugenol over Ru/C was quite minor above 50 bar. On the other hand, propylcyclohexane was the only product in eugenol HDO over carbon-supported CoN_x at 25 bar at 200 °C in 2 h, whereas the main product was dihydroeugenol at 5 bar.[20] This result was in accordance with the current results.

Regeneration and Reuse of IRA-1 Catalyst. The results from the reuse test of IRA-1 (Table 8, entries 10 and 11, Figure 10) showed that the initial TOF for transformation of dihydroeugenol was 7.5 fold higher when using a fresh catalyst and the initial isoeugenol concentration of 0.098 mol/L

DOI: 10.1021/acssuschemeng.8b03035
ACS Sustainable Chem. Eng. 2018, 6, 16205−16218

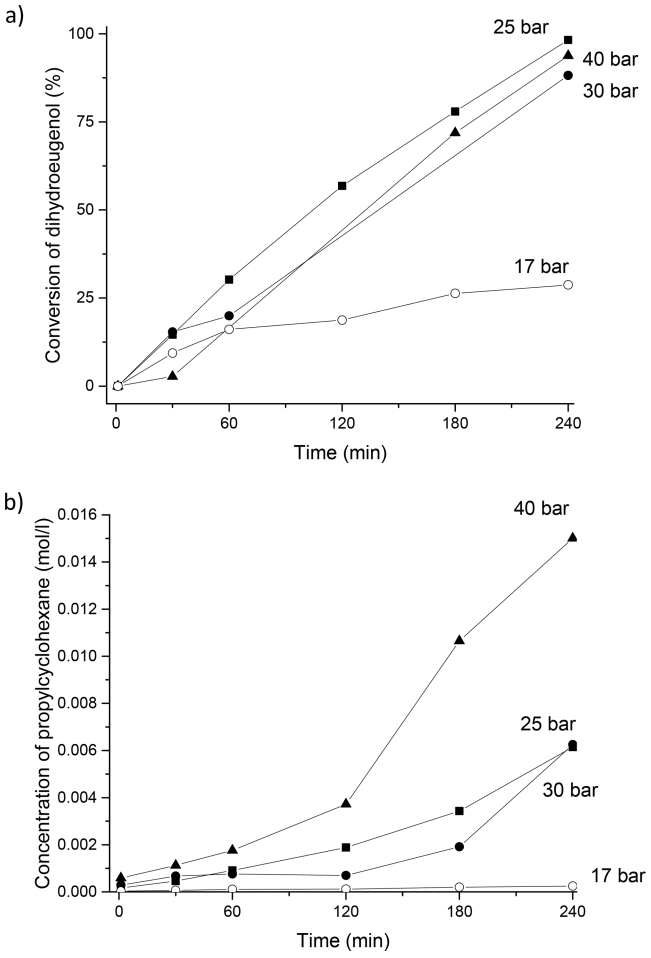

Figure 9. Effect of pressure in isoeugenol HDO using IRA-3 catalyst. (a) Conversion of dihydroeugenol and (b) concentration of propylcyclohexane (PCH) in HDO of isoeugenol at 250 °C under different pressures over IRA-3 catalyst. Notation: (o) 17 bar, (■) 25 bar, (●) 30 bar, and (▲) 40 bar.

compared to the case using 0.013 mol/L isoeugenol initial concentration and the regenerated catalyst, which is in line with the first-order kinetics (see above). This result indicates that the regenerated catalyst was initially quite active in transformation of dihydroeugenol but deactivated rapidly after 60 min. When the concentration of propylcyclohexane was plotted as a function of the concentration of dihydroeugenol, it can be seen that with the regenerated catalyst further transformations of dihydroeugenol stopped after the third sampling point after 60 min (Figure 10c). In our recent publication,[15] it was shown that hydrogenation of propylbenzene, which is an intermediate in isoeugenol HDO at 200 °C under 30 bar total pressure in hydrogen, is thermodynamically not feasible since the Gibbs free energy for that reaction was positive. The kinetic results, however, confirmed 75% yield of propylcyclohexane over Pt−H−Beta-300 showing that the reaction was kinetically controlled. Isoeugenol was converted with the fresh IRA-1 with 57% yield to propylcyclohexane. The regenerated IRA-1, tested in the second experiment with 0.013 mol/L initial concentration of isoeugenol, was not as active in HDO exhibiting only ca. 40% yield of propylcyclohexane. In addition also large amounts of dihydroeugenol (ca. 0.003 mol/L) were present. The spent catalyst does not possess the

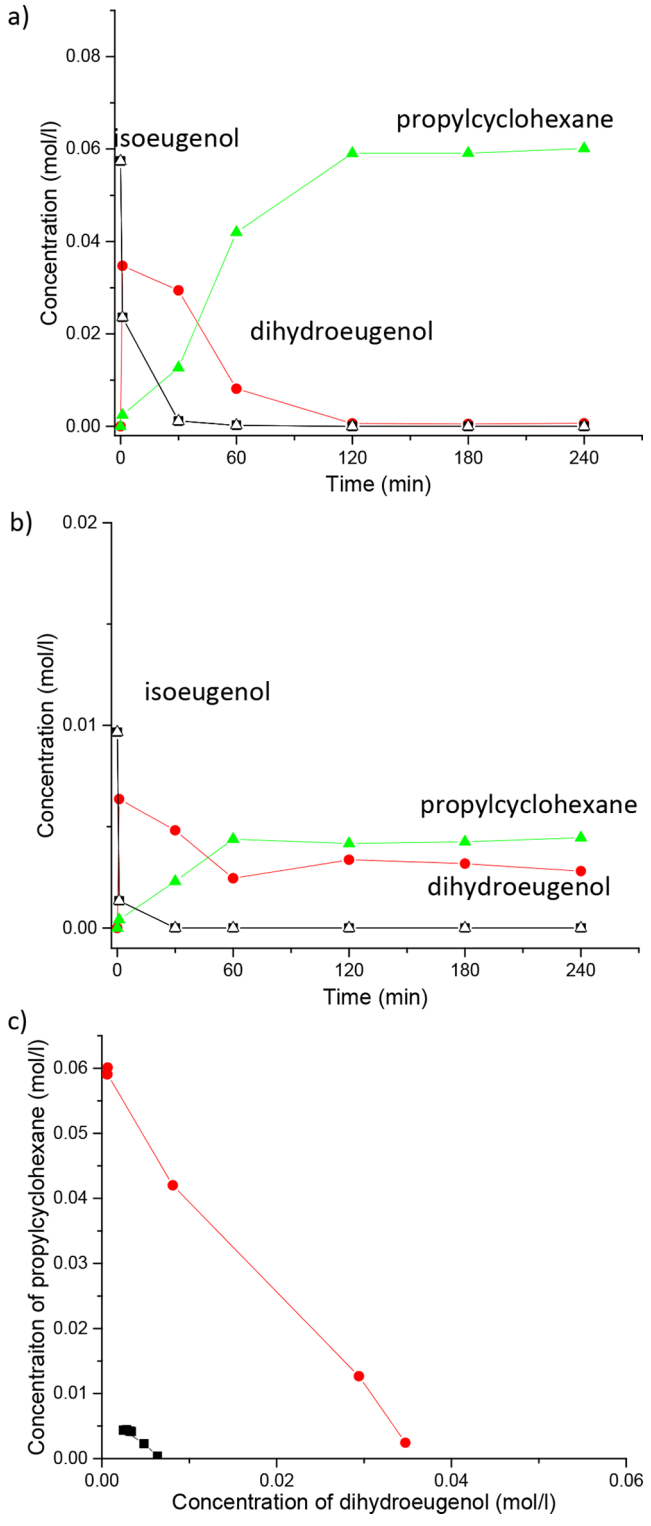

Figure 10. Concentration of isoeugenol and concentration of products (mol/L) vs reaction time (min) in isoeugenol HDO at 250 °C and 30 bar total pressure over (a) fresh and (b) spent and regenerated IRA-1 catalyst and (c) concentration of propylcyclohexane as a function of the concentration of dihydroeugenol. Symbols: (●) using initial concentration of isoeugenol of 0.098 mol/L and fresh catalyst, (■) initial concentration of isoeugenol 0.013 mol/L and spent, regenerated catalyst. Notation: (a) 0.4 g of fresh IRA-1 as a catalyst with the initial isoeugenol concentration 0.098 mol/L and (b) 0.05 g of the spent and regenerated IRA-1 catalyst using 0.013 mol/L isoeugenol, the weight ratio of reactant to catalyst in both cases 2.

DOI: 10.1021/acssuschemeng.8b03035
ACS Sustainable Chem. Eng. 2018, 6, 16205−16218

rhenium valence state of 4+ which can decrease its activity in HDO.

CONCLUSIONS

Hydrodeoxygenation (HDO) of isoeugenol was investigated at 200−250 °C under 17−40 bar hydrogen pressure for the first time using a range of mono- and bimetallic Pt, Ir, and Re catalysts in dodecane as a solvent. The catalysts were mainly prepared by the impregnation method, except one bimetallic Ir−Re/Al_2O_3, for which the deposition−precipitation method was applied. The bimetallic Ir−Re catalysts exhibited high metal dispersion according to TEM with the size close to 1 nm.

In HDO of isoeugenol over the Ir−Re/Al_2O_3 catalyst prepared by the deposition−precipitation method gave a complete conversion of isoeugenol with 69% yield of the desired product, propylcyclohexane, at 250 °C under hydrogen pressure 30 bar when using the reactant to catalyst ratio of 2 at the initial reactant concentration of 0.1 mol/L. Higher pressures strongly promoted HDO, and under 40 bar afforded formation of propylcyclohexane with 99% yield over Ir−Re/Al_2O_3 prepared by impregnation. The best catalyst, Ir−Re/Al_2O_3, prepared by the deposition precipitation was mildly acidic and according to XPS contained Re^{4+}.

ASSOCIATED CONTENT

Supporting Information

The Supporting Information is available free of charge on the ACS Publications website at DOI: 10.1021/acssuschemeng.8b03035.

Information as mentioned in the text. (PDF)

AUTHOR INFORMATION

Corresponding Author

*E-mail: dmurzin@abo.fi.

ORCID

Irina L. Simakova: 0000-0002-5138-4847

Dmitry Yu. Murzin: 0000-0003-0788-2643

Notes

The authors declare no competing financial interest.

ACKNOWLEDGMENTS

P. Paturi acknowledges the Jenny and Antti Wihuri Foundation for financial support. Funding for I. Simakova was provided through the Federal Project no. 0303-2016-0012 for the Boreskov Institute of Catalysis.

REFERENCES

(1) Xiu, S.; Shahbazi, A. Bio-oil production and upgrading research: A review. *Renewable Sustainable Energy Rev.* **2012**, *16*, 4406−4414.

(2) Demirbas, A. Current Technologies for the thermo-conversion of biomass into fuels and chemicals. *Energy Sources* **2004**, *26*, 715−730.

(3) Czernik, S.; Bridgwater, A. V. Overview of applications of biomass fast pyrolysis oil. *Energy Fuels* **2004**, *18*, 590−598.

(4) Wang, H.; Male, J.; Wang, Y. Recent advances in hydrotreating of pyrolysis bio-oil and its oxygen-containing model compounds. *ACS Catal.* **2013**, *3*, 1047−1070.

(5) Ghampson, I. T.; Sepulveda, C.; Garcia, R.; Fierro, J. L. G.; Escalona, N. Carbon nanofiber-supported ReOx catalysts for the hydrodeoxygenation of lignin-derived compounds. *Catal. Sci. Technol.* **2016**, *6*, 4356−4369.

(6) He, L.; Qin, Y.; Lou, H.; Chen, P. Highly dispersed molybdenum carbide nanoparticles supported on activated carbon as an efficient catalyst for the hydrodeoxygenation of vanillin. *RSC Adv.* **2015**, *5*, 43141−43147.

(7) De Souza, P. M.; Rabelo-Neto, R. C.; Borges, L. E. P.; Jacobs, G.; Davis, B. H.; Graham, U. M.; Resasco, D. E.; Noronha, F. B. Effect of zirconia morphology on hydrodeoxygenation of phenol over Pd/ZrO_2. *ACS Catal.* **2015**, *5* (12), 7385−7398.

(8) Gonzalez, C.; Marin, P.; Diez, F. V.; Ordonez, S. Gas phase hydrodeoxygenation of benzaldehyde, benzyl alcohol, phenylacetate and anisole over precious metal catalysts. *Ind. Eng. Chem. Res.* **2016**, *55*, 2319−2327.

(9) Mäki-Arvela, P.; Murzin, D. Hydrodeoxygenation of lignin-derived phenols: From fundamental studies towards industrial applications. *Catalysts* **2017**, *7* (9), 265.

(10) Shafaghat, H.; Rezaei, P. S.; Daud, W. M. A. W. Catalytic hydrodeoxygenation of simulated phenolic bio-oil to cycloalkanes and aromatic hydrocarbons over bifunctional metal/acid catalysts of Ni/HBeta, Fe/HBeta and NiFe/HBeta. *J. Ind. Eng. Chem.* **2016**, *35*, 268−276.

(11) Deepa, A. K.; Dhepe, P. L. Function of metals and supports on the hydrodeoxygenation of phenolic compounds. *ChemPlusChem* **2014**, *79*, 1573−1583.

(12) Lyu, G.; Wu, S.; Zhang, H. Estimation and comparison of bio-oil components from different pyrolysis conditions. *Front. Energy Res.* **2015**, *3*, 1−11.

(13) Bjelić, A.; Grilc, M.; Likozar, B. Catalytic hydrogenation and hydrodeoxygenation of lignin-derived model compound eugenol over Ru/C: Intrinsic microkinetics and transport phenomena. *Chem. Eng. J.* **2018**, *333*, 240−259.

(14) Zhang, X.; Zhang, Q.; Wang, T.; Ma, L.; Yu, Y.; Chen, L. Hydrodeoxygenation of lignin-derived phenolic compounds to hydrocarbons over Ni/SiO_2−ZrO_2 catalysts. *Bioresour. Technol.* **2013**, *134*, 73−80.

(15) Bomont, L.; Alda-Onggar, M.; Fedorov, V.; Aho, A.; Peltonen, J.; Eränen, K.; Peurla, M.; Kumar, N.; Russo, V.; Mäki-Arvela, P.; Grenman, H.; Lindblad, M.; Murzin, D. Yu.; Warna, J. Production of cycloalkanes in hydrodeoxygenation of isoeugenol over Pt- and Ir-modified bifunctional catalysts. *Eur. J. Inorg. Chem.* **2018**, *2018*, 2841.

(16) Li, X.; Xing, J.; Zhou, M.; Zhang, H.; Huang, H.; Zhang, C.; Song, L.; Li, X. Influence of crystal size of HZSM-5 on hydrodeoxygenation of eugenol in aqueous phase. *Catal. Commun.* **2014**, *56*, 123−127.

(17) Jung, K. B.; Lee, J.; Ha, J.-M.; Lee, H.; Suh, D. J.; Jun, X.-H.; Jae, J. Effective hydrodeoxygenation of lignin-derived phenols using bimetallic RuRe catalysts: Effect of carbon supports. *Catal. Today* **2018**, *303*, 191−199.

(18) Feng, J.; Hse, C.-Y.; Yang, Z.; Wang, K.; Jiang, J.; Xu, J. Liquid phase in situ hydrodeoxygenation of biomass-derived phenolic compounds to hydrocarbons over bifunctional catalysts. *Appl. Catal., A* **2017**, *542*, 163−173.

(19) Qi, J.; Sun, X.; Tang, S.-F.; Sun, Y.; Li, X.; Li, X.; Xu, C. Integrated study on the role of solvent, catalyst and reactant in the hydrodeoxygenation of eugenol over nickel based catalysts. *Appl. Catal., A* **2017**, *535*, 24−31.

(20) Liu, X.; Jia, W.; Xu, G.; Zhang, Y.; Fu, Y. Selective hydrodeoxygenation of lignin-derived phenols to cyclohexanols over Co-based catalysts. *ACS Sustainable Chem. Eng.* **2017**, *5*, 8594−8601.

(21) Zhang, X.; Tang, W.; Zhang, Q.; Wang, T.; Ma, L. Hydrocarbons production from lignin-derived phenolic compounds over Ni/SiO_2 catalyst. *Energy Procedia* **2017**, *105*, 518−523.

(22) Zhang, C.; Xing, J.; Song, L.; Xin, H.; Lin, S.; Xing, L.; Li, X. Aqueous-phase hydrodeoxygenation of lignin monomer eugenol: Influence of Si/Al ratio of H->ZSM-5 on catalytic perfomances. *Catal. Today* **2014**, *234*, 145−152.

(23) Lam, E.; Luong, J. H. T. Carbon materials as catalyst supports and catalysts in the transformation of biomass to fuels and chemicals. *ACS Catal.* **2014**, *4* (10), 3393−3410.

(24) Liu, S.; Dutta, S.; Zheng, W.; Gould, N. S.; Cheng, Z.; Xu, B.; Saha, B.; Vlachos, D. G. Catalytic hydrodeoxygenation of high carbon

furylmethanes to renewable jet-fuel ranged alkanes over a rhenium-modified iridium catalyst. *ChemSusChem* **2017**, *10*, 3225−4234.
(25) Chen, K.; Mori, K.; Watanabe, H.; Nakagawa, Y.; Tomishige, K. C−O bond hydrogenolysis of cyclic ethers with OH groups over rhenium-modified supported iridium catalysts. *J. Catal.* **2012**, *294*, 171−183.
(26) Amada, Y.; Shinmi, Y.; Koso, S.; Kubota, T.; Nakagawa, Y.; Tomishige, K. Reaction mechanism of the glycerol hydrogenolysis to 1,3-propanediol over Ir−ReOx/SiO_2 catalyst. *Appl. Catal., B* **2011**, *105*, 117−127.
(27) Tamura, M.; Tokonami, K.; Nakagawa, Y.; Tomishige, K. Rapid synthesis of unsaturated alcohols under mild conditions by highly selective hydrogenation. *Chem. Commun.* **2013**, *49*, 7034−7036.
(28) Emeis, C. A. Determination of integrated molar extinction coefficients for infrared absorption bands of pyridine adsorbed on solid acid catalysts. *J. Catal.* **1993**, *141*, 347−354.
(29) Delidovich, I. V.; Taran, O. P.; Matvienko, L. G.; Simonov, A. N.; Simakova, I. L.; Bobrovskaya, A. N.; Parmon, V. N. Selective oxidation of glucose over carbon-supported Pd and Pt catalysts. *Catal. Lett.* **2010**, *140*, 14−21.
(30) Abdullah, H. A.; Hauser, A.; Ali, F. A.; Al-Adwani, A. Optimal conditions for coke extraction of spent catalysts by accelerated solvent extraction compared to Soxhlet. *Energy Fuels* **2006**, *20*, 320−323.
(31) Gutsche, C.; Moeller, C. J.; Knipper, M.; Borchert, H.; Parisi, J.; Plaggenborg, T. Synthesis, structure, and electrochemical stability of Ir-decorated RuO_2, nanoparticles and Pt nanorods as oxygen catalysts. *J. Phys. Chem. C* **2016**, *120*, 1137−1146.
(32) Lejaeghere, K.; Van Speybroeck, V.; Van Oost, G.; Cottenier, S. Error estimates for solid-state density-functional theory predictions: an overview by means of the ground-state elemental crystals. *Crit. Rev. Solid State Mater. Sci.* **2014**, *39*, 1−24.
(33) Bannikov, V. V.; Shein, I. R.; Ivanovskii, A. L. Elastic and electronic properties of hexagonal rhenium sub-nitrides Re_3N and Re_2N in comparison with hcp-Re and wurtzite-like rhenium mononitride. *Phys. Status Solidi B* **2011**, *248*, 1369−1374.
(34) Ivanovskii, A. L.; Chupakhina, T. I.; Zubkov, V. G.; Tyutyunnik, A. P.; Krasilnikov, V. N.; Bazuev, G. V.; Okatov, S. V.; Lichtenstein, A. I. Structure and electronic properties of new rutile-like rhenium(IV) dioxide ReO_2. *Phys. Lett. A* **2005**, *348*, 66−70.
(35) Samain, L.; Jaworski, A.; Edén, M.; Ladd, D. M.; Seo, D. K.; Garcia-Garcia, F. J.; Häussermann, U. Structural analysis of highly porous γ-Al_2O_3. *J. Solid State Chem.* **2014**, *217* (36), 1−8.
(36) Kip, B. J.; Van Grondelle, J. H. A.; Prins, R.; Martens, J. H. A. Preparation and characterization of very highly dispersed iridium on Al_2O_3 and SiO_2. *Appl. Catal.* **1986**, *26*, 353−373.
(37) Hilmen, A. M.; Schanke, D.; Holmen, A. TPR study of the mechanism of rhenium promotion of alumina-supported cobalt Fischer−Tropsch catalysts. *Catal. Lett.* **1996**, *38*, 143−147.
(38) Paz, D. S.; Damyanova, S.; Borges, L. R.; Santos, J.H. B. O.; Bueno, J. M. C. Identifying the adsorbed active intermediates on Pt surface and promotion of activity through the redox CeO_2 in preferential oxidation of CO in H_2. *Appl. Catal., A* **2017**, *548*, 164−178.
(39) Wagstaff, N.; Prins, R. Alloy formation and metal oxide segregation in Pt-Re/γ-Al_2O_3 catalysts as investigated by temperature-programmed reduction. *J. Catal.* **1979**, *59*, 434−445.
(40) Webb, A. Reducibility of supported rhenium. *J. Catal.* **1975**, *39*, 485−487.
(41) Freakley, S. J.; Ruiz-Esquius, J.; Morgan, D. J. The X-ray photoelectron spectra of Ir, IrO_2 and $IrCl_3$ revisited. *Surf. Interface Anal.* **2017**, *49*, 794−799.
(42) Salnikov, O. G.; Burueva, D. B.; Gerasimov, E.Yu; Bukhtiyarov, A. V.; Khudorozhkov, A. K.; Prosvirin, I. P.; Kovtunova, L. M.; Barskiy, D. A.; Bukhtiyarov, V. I.; Kovtunov, K. V.; Koptyug, I. V. The effect of oxidative and reductive treatments of titania-supported metal catalysts on the pairwise hydrogen addition to unsaturated hydrocarbons. *Catal. Today* **2017**, *283*, 82−88.
(43) Bernas, H.; Simakova, I.; Mäki-Arvela, P.; Prosvirin, I. P.; Leino, R.; Murzin, D.Yu. Hydrogenation of citral over carbon supported iridium catalysts. *Catal. Lett.* **2012**, *142*, 690−697.
(44) Shpiro, E. S.; Ryashentseva, M. A.; Minachev, K. M.; Antoshin, G. V.; Avaev, V. I. XPS studies of the rhenium state in supported rhenium catalysts. *J. Catal.* **1978**, *55*, 402−406.
(45) Rozmysłowicz, B.; Kirilin, A.; Aho, A.; Manyar, H.; Hardacre, C.; Wärnå, J.; Salmi, T.; Murzin, D. Yu. Selective hydrogenation of fatty acids to alcohols over highly dispersed ReOx/TiO_2 catalyst. *J. Catal.* **2015**, *328*, 197−207.
(46) Pamphile-Adrián, A. J.; Florez-Rodriguez, P. P.; Passos, F. B. Iridium catalysts for C-C hydrogenolysis: Catalytic consequences of iridium sites. *J. Braz. Chem. Soc.* **2015**, *27* (5), 958−966.
(47) Jongerius, A. L.; Gosselink, R. W.; Dijkstra, J.; Bitter, J. H.; Bruijnincx, P. C. A.; Weckhuysen, B. M. Carbon nanofiber supported transition-metal carbide catalysts for the hydrodeoxygenation of guaiacol. *ChemCatChem* **2013**, *5*, 2964−2972.

DOI: 10.1021/acssuschemeng.8b03035
ACS Sustainable Chem. Eng. 2018, 6, 16205−16218